

DISCOVERY OF SUPERTHERMAL HYDROXYL (OH) IN THE HH 211 OUTFLOW

A. TAPPE¹, C. J. LADA¹, J. H. BLACK², A. A. MUENCH¹

Preprint: accepted by ApJ Letters, May 12, 2008

ABSTRACT

We present a 5–37 μm infrared spectrum obtained with the *Spitzer Space Telescope* toward the southeastern lobe of the young protostellar outflow HH 211. The spectrum shows an extraordinary sequence of OH emission lines arising in highly excited rotational levels up to an energy $E/k \approx 28200\text{K}$ above the ground level. This is, to our knowledge, by far the highest rotational excitation of OH observed outside Earth. The spectrum also contains several pure rotational transitions of H_2O ($v = 0$), H_2 ($v = 0$) S(0) to S(7), HD ($v = 0$) R(3) to R(6), and atomic fine-structure lines of [Fe II], [Si II], [Ne II], [S I], and [Cl I]. The origin of the highly excited OH emission is most likely the photodissociation of H_2O by the UV radiation generated in the terminal outflow shock of HH 211.

Subject headings: ISM: Herbig-Haro objects — ISM: individual (HH 211) — ISM: jets and outflows — ISM: molecules — shock waves

1. INTRODUCTION

OH and H_2O are molecules of central importance to the interstellar oxygen chemistry in many diverse environments ranging from interstellar clouds to protoplanetary disks and comets, and they act as important shock coolants due to their rich infrared spectra (e.g. Hollenbach & McKee 1979; Draine et al. 1983; Neufeld & Dalgarno 1989; Hollenbach & McKee 1989; Wardle 1999). The potential pathways leading to the formation and destruction of these molecules are now believed to be well established. However, the relative importance of these pathways in a given astrophysical environment is generally poorly constrained due to a lack of suitable observations and the complex interaction of formation, destruction, and excitation mechanisms for H_2O and OH.

Both molecules are expected to be formed in abundance in hot molecular gas ($T \gtrsim 1000\text{K}$) owing to a series of neutral-neutral reactions whose activation barriers are overcome at high temperatures. *ISO* (Infrared Space Observatory), *SWAS* (Submillimeter Wave Astronomy Satellite), and *Odin* observations show enhanced OH and H_2O abundances in stellar outflows (e.g. Giannini et al. 2001, Benedettini et al. 2002, Lerate et al. 2006, Persson et al. 2007, and Franklin et al. 2008). However, the large beam sizes prevented a detailed spatial analysis, which is essential to investigate the OH and H_2O formation processes that lead to the increased abundances. In addition, the submillimeter observations of H_2O are mostly confined to the $1_{10}\text{--}1_{01}$ transition of ortho- H_2O at 556.9 GHz ($E/k = 61\text{K}$), and the wavelength coverage of the *ISO* Long Wavelength Spectrometer (LWS) limited observations of OH to rotational states with $E/k < 1200\text{K}$.

In this paper, we present the first detection of rotationally excited OH at previously unobserved high excitation levels up to $E/k \approx 28200\text{K}$ in HH 211 with the *Spitzer Space Telescope* (Werner et al. 2004).

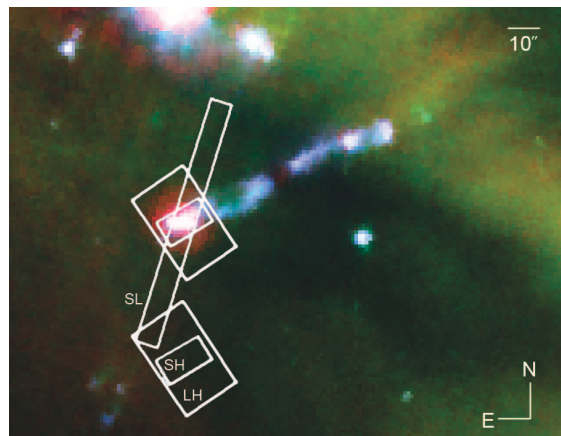


FIG. 1.— HH 211: *Spitzer* IRAC 3–9 μm +MIPS 24 μm color composite image (3.6+4.5 μm =blue, 8.0 μm =green, and 24 μm =red). White boxes outline the IRS SL, SH, and LH map coverage including the SH/LH background position. The image center coordinates are $3^{\text{h}}43^{\text{m}}56^{\text{s}}.8$, $32^{\circ}00'34''.4$ (J2000).

HH 211, one of the youngest known stellar outflows, is highly collimated, of extremely high velocity (EHV; jet speed of $100\text{--}300\text{kms}^{-1}$ assuming an inclination of 5 to 10° with respect to the plane of the sky, see O’Connell et al. 2005 and Lee et al. 2007), bipolar, and associated with a Class 0 protostar in the young stellar cluster IC 348. It has been studied in detail via excited H_2 , CO, and SiO (e.g. McCaughrean et al. 1994; Gueth & Guilloteau 1999; Eislöffel et al. 2003; O’Connell et al. 2005; Caratti o Garatti et al. 2006; Tafalla et al. 2006; Lee et al. 2007). The unique combination of sensitivity, wavelength coverage, and mapping capabilities with *Spitzer* enables us to study the spatial structure of the HH 211 outflow bow-shock and to investigate the regions of shock-induced OH and H_2O formation.

2. OBSERVATIONS AND DATA REDUCTION

HH 211 was observed with the *Spitzer* Infrared Spectrograph (IRS, Houck et al. 2004) on 2007 March 12. We mapped the outermost region of the southeastern outflow lobe using the IRS short-low (SL2/SL1, 5.2–8.7/7.4–14.5 μm), short-high (SH, 9.9–19.6 μm), and long-high

¹ Harvard-Smithsonian Center for Astrophysics, 60 Garden Street, MS-72, Cambridge, MA 02138; atappe@cfa.harvard.edu

² Onsala Space Observatory, Chalmers University of Technology, SE-43992 Onsala, Sweden

(LH, 18.7–37.2 μm) modules. The nominal spectral resolution is $R = 64$ –128 as a function of wavelength for the low resolution and $R = 600$ for the high resolution settings. The total exposure times were 588 s for each SL, 720 s for the SH, and 600 s for the LH module. We also obtained IRAC (Infrared Array Camera, Fazio et al. 2004) and MIPS (Multiband Imaging Photometer for Spitzer, Rieke et al. 2004) image mosaics of HH 211 from the *Spitzer* data archive.

We performed the IRS data reduction consisting of background subtraction, masking of bad pixels, extracting the spectra, and generating the spectral line maps with CUBISM v1.50 (Smith et al. 2007). We applied CUBISM’s slit-loss correction function, and expect the absolute flux calibration of our spectrum to be accurate within 20%. A calibration to the observed MIPS 24 μm photometry is unreliable due to the strong line emission and the more than 2 year time difference between our IRS and the archival MIPS observations.

3. RESULTS

The spectrum of HH 211 displayed in Figure 2 reveals a sequence of highly excited OH ($v = 0$, $J' \rightarrow J' - 1$) pure rotational transitions arising in the ${}^2\Pi_{3/2}$ and ${}^2\Pi_{1/2}$ rotational ladders from $J' = 15/2$ to $69/2$, which result in closely spaced doublets that become partly resolvable only at wavelengths greater than 20 μm in our spectra. An additional splitting due to Λ -doubling is only barely noticeable for the OH lines at the longest wavelengths in our spectra (see Herzberg 1971, for a detailed treatment of OH spectroscopy). The OH energy level diagram in Figure 3 shows that the highest excited OH transition has an upper state energy of $E/hc = 19607\text{ cm}^{-1}$ ($E/k \approx 28200\text{ K}$) above the ground level. Note that the population of the OH energy levels probably extends to even higher energies, but the corresponding rotational transitions fall in the wavelength range of the low resolution IRS modules below 10 μm . Due to the lower resolution, the SL modules are not sensitive enough to detect the faint, narrow emission lines.

In addition, there are OH cross-ladder transitions with $\Delta J = 0, +1$, but all such transitions that fall in the 5–37 μm region have transition probabilities orders of magnitude smaller than the intra-ladder transitions described above. Nevertheless, we detect the two lowest excited OH ($v = 0$, ${}^2\Pi_{1/2} \rightarrow {}^2\Pi_{3/2}$, $J' \rightarrow J' - 1$) cross-ladder transitions with upper levels $J' = 7/2$ and $5/2$ ($E/k \approx 620$ and 420 K) at 28.94 and 34.62 μm (see Fig. 2), respectively, indicating a substantial population in the lower OH J -levels. We did not unambiguously detect any pure rotational OH transitions from excited vibrational levels.

The low resolution portion of the spectrum is dominated by the strong, pure rotational H₂ (0–0) S(3)–S(7) transitions and the much weaker [Fe II] 5.34 μm line. In addition to the previously mentioned OH lines, the high resolution portion longward of 10 μm shows H₂ (0–0) S(0)–S(2) including (1–1) S(3) at 10.18 μm , HD (0–0) R(3)–R(6), numerous H₂O ($v = 0$) pure rotational lines, and forbidden atomic fine-structure lines from [Fe II], [Si II], [Ne II], [S I], and [Cl I]. The spectrum also has noticeable continuum emission longward of 15 μm , which can be fitted by thermal dust emission at a temperature $\sim 85\text{ K}$, represented by a modified blackbody with the dust emissivities of Weingartner & Draine

(2001). Two additional components at about 170 K and 30 K are needed to fit the complete continuum including the 8–15 μm region and the MIPS 70 μm flux of $F_\lambda = 1.1 \times 10^{-16}\text{ W m}^{-2}\mu\text{m}^{-1}$. There is also a strongly rising continuum shortward of 8 μm . The peculiar NIR continuum of HH 211 was previously noted by Eislöffel et al. (2003) and confirmed by O’Connell et al. (2005), who interpret it as scattered light from the protostar escaping along the low-density jet cavity.

4. DISCUSSION

4.1. The origin of high- J OH emission

In §3, we reported the detection of rotationally excited OH at previously unobserved high excitation levels in HH 211. As a consequence of the large OH dipole moment, the observed intra-ladder pure rotational transitions have large Einstein A -coefficients of the order of 10 to 400 s^{-1} . For comparison, our observed pure rotational H₂O transitions have $A \sim 1$ – 20 s^{-1} , the [Fe II] lines have A -values of a few 10^{-3} s^{-1} , and the H₂ S(0)–S(7) pure rotational lines have A -values between 3×10^{-7} and $3 \times 10^{-11}\text{ s}^{-1}$. Large A -values make collisional excitation of high energy levels very ineffective at lower densities, i.e. the corresponding critical densities are usually much larger than the gas density. The observed OH lines in HH 211 demonstrate that energy levels up to at least $E/k \approx 28200\text{ K}$ are well populated despite the large OH A -values. This fact, coupled with the observed distribution of OH line intensities, strongly suggests a selective, non-thermal origin of the high- J OH excitation. For comparison, a non-LTE analysis of the [Fe II] lines in our spectrum suggests a gas temperature less than a few 1000 K. Furthermore, all of our observed pure rotational H₂O lines originate from energy levels with $E/k < 2400\text{ K}$ even though there are many pure rotational H₂O transitions with $A \sim 50$ – 100 s^{-1} from energy levels between 3000 and 8000 K in the 10–38 μm wavelength range.

Theoretical and experimental laboratory studies show that OH molecules produced via photodissociation of H₂O at photon energies larger than about 9 eV ($\lambda < 140\text{ nm}$) are mostly in the ground electronic and vibrational state but with a high rotational excitation favoring $J = 70/2$ to $90/2$ with $E/k \gtrsim 30000\text{ K}$ (Mordaunt et al. 1994; van Harrevelt & van Hemert 2000; Harich et al. 2000). This is because the absorption of UV radiation in the H₂O (\tilde{B} – \tilde{X}) band produces OH in an excited electronic state, $A\ ^2\Sigma^+$, which, in turn, efficiently yields highly excited ground-state OH ($X\ ^2\Pi$) molecules via a nonadiabatic crossing between intersecting potential energy surfaces (see van Harrevelt & van Hemert 2000; Harich et al. 2000). This process leads to a highly selective formation of high- J OH in the ground electronic and vibrational state, followed by a radiative cascade down the rotational ladders depicted in Fig. 3. This is consistent with our observed distribution of OH line intensities and our non-detection of OH pure rotational transitions from excited vibrational states. We will present a detailed non-LTE excitation model of OH, H₂O, and H₂ together with an analysis of the atomic fine-structure transitions in a subsequent paper.

Further evidence for the role of H₂O photodissociation as a source of high- J OH can be gained from spatial mapping of the emission lines. Our *Spitzer* IRS

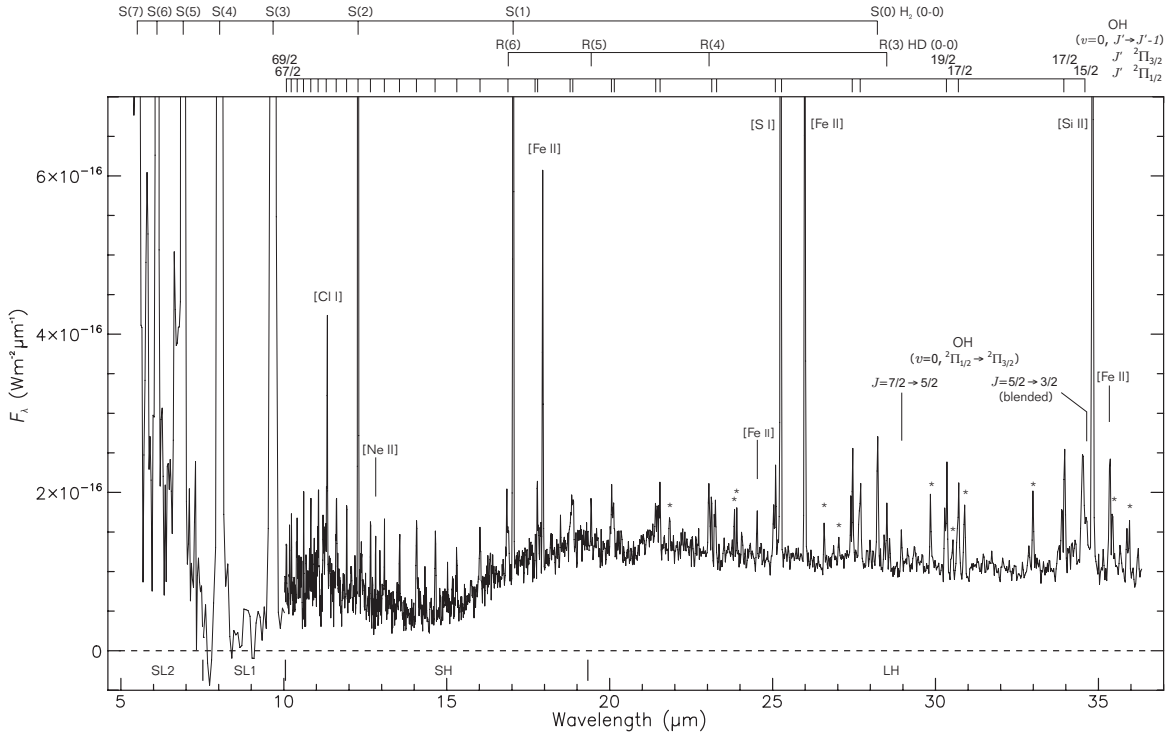


FIG. 2.— Background subtracted *Spitzer* IRS spectrum of HH 211: all major detected lines are labelled, and the strongest H₂O lines are marked with an asterisk. The strongest lines are clipped for illustration purposes.

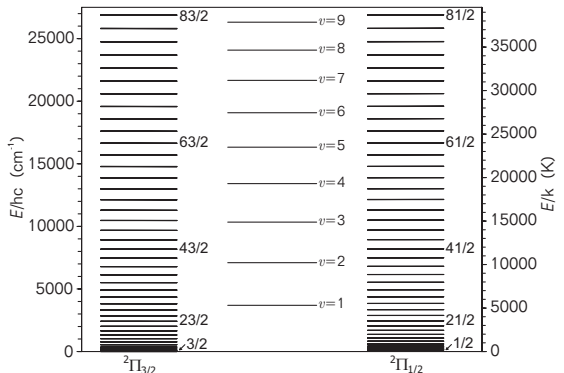


FIG. 3.— OH ($X^2\Pi, v=0$) rotational energy levels. The two rotational ladders result from the spin-orbit coupling of the unpaired $2p$ electron. All rotational levels are further split into Λ -type doublets with separations between 0.1 and 35.0 cm^{-1} , which are not visible on the scale of this plot (data from Colin et al. 2002).

maps cover the southeastern terminal shock of HH 211, which exhibits a typical bow-shock geometry in H₂ and CO emission (Gueth & Guilloteau 1999; Eisloffel et al. 2003). Figure 4 shows the spatial distribution of rotationally excited OH and H₂O together with the $25\text{ }\mu\text{m}$ dust continuum surface brightness. The highly localized optical H α emission (Walawender et al. 2006) is practically coincident with the $25\text{ }\mu\text{m}$ surface brightness maximum. Their emission maxima are offset by about $1''$, which is within the positional map accuracy (see Fig. 4). This region is located at the bow-shock apex, where the shock velocity is expected to be the highest and presumably most of the shock generated FUV radiation originates. The emission maximum of rotationally excited OH (Fig. 4, left map) also coincides with the bow shock apex. Although not shown in Figure 4 due to the limited spatial coverage, the emission maximum of the OH

($J' > 29/2$) rotational lines in the SH wavelength range occurs at the same location. However, unlike H α , the continuum, OH, and H₂O emission clearly extend well beyond the bow shock. Using the $25\text{ }\mu\text{m}$ continuum surface brightness as a surrogate tracer of the UV radiation field, we clearly note the presence of a radiative precursor upstream of the shock. Note that although collisional grain heating due to inelastic gas-grain collisions may contribute to the dust heating in the bow shock, it is probably unimportant outside and ahead of the shock.

4.1.1. Formation of OH and H₂O

Our emission line maps show clear evidence of OH and H₂O emission in the precursor region (see Fig. 4). It is unlikely that the chemical formation route via $\text{H}_2 + \text{O} \rightarrow \text{OH} + \text{H}$ and $\text{H}_2 + \text{OH} \rightarrow \text{H}_2\text{O} + \text{H}$ (e.g. Hollenbach & McKee 1979; Neufeld & Dalgarno 1989) is the dominant source of OH and H₂O in the UV precursor upstream of the shock. These reactions have significant Arrhenius activation energies (E_A/k about 3150 and 1736 K, respectively) and only proceed efficiently in dense, hot gas. The absence of rovibrational H₂ emission in the preshock region confirms the absence of hot, shocked gas needed to directly form OH and H₂O through gas chemistry.

Instead, we propose that UV induced photodesorption of water ice from grain mantles and photodissociation of H₂O either in the gas phase or directly in the grain ice mantles (see Andersson et al. 2006) are the primary sources of OH and H₂O in the precursor. We evaluated the H₂O photodesorption rate using the Ly α dominated FUV emission generated by a shock with a speed of $v_s = 40\text{ km s}^{-1}$ and a preshock density of $n_0 = 10^3\text{--}10^4\text{ cm}^{-3}$ (atomic shock models by J. Raymond, private communication). Such a shock approximately reproduces our observed [Ne II] 12.8, [S I] 25.2,

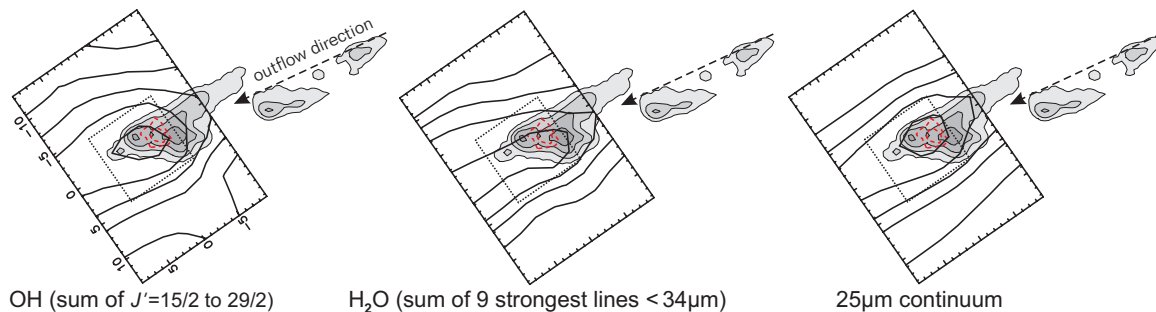


FIG. 4.— *Spitzer* IRS LH emission line maps of HH 211 (solid lines) overlaid on the $\text{H}_2(1-0) S(1) 2.12 \mu\text{m}$ (shaded contours; Eisloffel et al. 2003) and optical $\text{H}\alpha$ emission (red, dashed contours; Walawender et al. 2006). Coordinates are in arcseconds offset from the (0,0) center. The maps are interpolated to half the original LH pixel size of $4.5''$, and the positional accuracy is $\sim 1''$. The dotted box marks the extracted region of the LH spectrum in Fig. 2. The linearly spaced max/min levels for the OH and H_2O emission contours going outwards from the center are $5.2/1.2 \times 10^{-8}$ and $1.0/0.2 \times 10^{-8} \text{ W m}^{-2} \text{ sr}^{-1}$, and $13/2 \text{ MJy sr}^{-1}$ for the $25 \mu\text{m}$ continuum.

[Fe II] 26.0 , and [Si II] $34.8 \mu\text{m}$ emission line intensities, which are good indicators for v_s and n_0 (see e.g. Fig. 7 in Hollenbach & McKee 1989). Our estimate shows that grain ice mantles can be efficiently removed via photodesorption on timescales of the order of 10^3 yr assuming the experimentally measured $\text{Ly}\alpha$ photodesorption yield for water ice of $3-5 \times 10^{-3}$ molecules per photon and a $\text{Ly}\alpha$ photodesorption cross section $\sim 8 \times 10^{-18} \text{ cm}^{-2}$ per individual water ice molecule (Westley et al. 1995a,b). This is consistent with the estimate of Hollenbach & McKee (1979), who argued that a shock with $v_s \gtrsim 40 \text{ km s}^{-1}$ would lead to complete upstream photodesorption of grain ice mantles assuming a photodesorption yield of 5×10^{-3} . At the high visual extinction toward the terminal shock of the HH 211 southeastern lobe, $A_V \approx 12 \pm 3 \text{ mag}$ (O’Connell et al. 2005; Caratti o Garatti et al. 2006), most of the gas phase water would otherwise be expected to reside frozen onto grains (cf. Melnick & Bergin 2005).

It is interesting to compare our observation of HH 211 with a recent *Spitzer* IRS detection of strong water emission toward the protostellar object IRAS 4B in NGC 1333 by Watson et al. (2007). These authors attribute the origin of this emission to the very dense, warm molecular layer of a protoplanetary disk. In this case, the main source of water is probably thermal sublimation of grain ice mantles in the $\sim 170 \text{ K}$ warm surface layer as suggested by Watson et al. (2007). Sublimation is insignificant at grain temperatures below about 100 K (cf. the derived dust temperature of $\sim 85 \text{ K}$ in HH 211 from our

dust continuum fit, see §3), but it becomes rapid above 120 K (see Fraser et al. 2001, Table 2). In addition to the strong H_2O emission, we have subsequently identified OH emission limited to transitions with $J' < 21/2$ ($E/k < 3500 \text{ K}$) in the IRS LH spectrum of IRAS 4B by reanalyzing the *Spitzer* archival spectra originally published by Watson et al. (2007). The comparatively low excitation of OH indicated by the absence of lines with $J' = 23/2$ to $27/2$ and the weakness of the OH emission relative to H_2O in IRAS 4B are consistent with the proposed sublimation origin of water and suggest that FUV photodissociation of H_2O plays only a minor role compared to HH 211.

This work is based on observations made with the *Spitzer* Space Telescope, which is operated by the Jet Propulsion Laboratory, California Institute of Technology under a contract with NASA. Support for this work was provided by NASA, by a *Spitzer* GO grant (JPL #1288815), and by the Swedish Research Council. We thank J. Eisloffel, D. Froebrich, and K.-W. Hodapp for providing the near-IR H_2 data, J. Walawender for the optical $\text{H}\alpha$ data used in Fig. 4, and J. Raymond for providing shock model results and useful discussions. Furthermore, we thank D. Neufeld for informative discussions, in particular, for calling our attention to the laboratory experiments of H_2O photodissociation and for suggesting the possible relevance of the OH excitation mechanism through H_2O photodissociation for HH 211.

REFERENCES

- Andersson, S., Al-Halabi, A., Kroes, G.-J., & van Dishoeck, E. F. 2006, *J. Chem. Phys.*, 124, 4715
- Benedettini, M., Viti, S., Giannini, T., et al. 2002, *A&A*, 395, 657
- Caratti o Garatti, A., Giannini, T., Nisini, B., & Lorenzetti, D. 2006, *A&A*, 449, 1077
- Colin, R., Coheur, P.-F., Kiseleva, M., Vandaele, A. C., & Bernath, P. F. 2002, *J. Mol. Spec.*, 214, 225
- Draine, B. T., Roberge, W. G., & Dalgarno, A. 1983, *ApJ*, 264, 485
- Eisloffel, J., Froebrich, D., Stanke, T., & McCaughrean, M. J. 2003, *ApJ*, 595, 259
- Fazio, G. G., Hora, J. L., Allen, L. E., et al. 2004, *ApJS*, 154, 10
- Franklin, J., Snell, R. L., Kaufman, M. J., et al. 2008, *ApJ*, 674, 1015
- Fraser, H. J., Collings, M. P., McCoustra, M. R. S., & Williams, D. A. 2001, *MNRAS*, 327, 1165
- Giannini, T., Nisini, B., & Lorenzetti, D. 2001, *ApJ*, 555, 40
- Gueth, F. & Guilloteau, S. 1999, *A&A*, 343, 571
- Harich, S. A., Hwang, D. W. H., Yang, X., et al. 2000, *J. Chem. Phys.*, 113, 10073
- Herzberg, G. 1971, *The spectra and structures of simple free radicals. An introduction to molecular spectroscopy* (Cornell University Press)
- Hollenbach, D. & McKee, C. F. 1979, *ApJS*, 41, 555
- Hollenbach, D. & McKee, C. F. 1989, *ApJ*, 342, 306
- Houck, J. R., Roellig, T. L., van Cleve, J., et al. 2004, *ApJS*, 154, 18
- Lee, C.-F., Ho, P. T. P., Palau, A., et al. 2007, *ApJ*, 670, 1188
- Lerate, M. R., Barlow, M. J., Swinyard, B. M., et al. 2006, *MNRAS*, 370, 597
- McCaughrean, M. J., Rayner, J. T., & Zinnecker, H. 1994, *ApJ*, 436, L189
- Melnick, G. J. & Bergin, E. A. 2005, *Advances in Space Research*, 36, 1027
- Mordaunt, D. H., Ashfold, M. N. R., & Dixon, R. N. 1994, *J. Chem. Phys.*, 100, 7360
- Neufeld, D. A. & Dalgarno, A. 1989, *ApJ*, 340, 869

- O'Connell, B., Smith, M. D., Froebrich, D., Davis, C. J., & Eisloffel, J. 2005, *A&A*, 431, 223
- Persson, C. M., Olofsson, A. O. H., Koning, N., et al. 2007, *A&A*, 476, 807
- Rieke, G. H., Young, E. T., Engelbracht, C. W., et al. 2004, *ApJS*, 154, 25
- Smith, J. D. T., Armus, L., Dale, D. A., et al. 2007, *PASP*, 119, 1133
- Tafalla, M., Kumar, M. S. N., & Bachiller, R. 2006, *A&A*, 456, 179
- van Harrevelt, R. & van Hemert, M. C. 2000, *J. Chem. Phys.*, 112, 5787
- Walawender, J., Bally, J., Kirk, H., et al. 2006, *AJ*, 132, 467
- Wardle, M. 1999, *ApJ*, 525, L101
- Watson, D. M., Bohac, C. J., Hull, C., et al. 2007, *Nature*, 448, 1026
- Weingartner, J. C. & Draine, B. T. 2001, *ApJ*, 548, 296
- Werner, M. W., Roellig, T. L., Low, F. J., et al. 2004, *ApJS*, 154, 1
- Westley, M. S., Baragiola, R. A., Johnson, R. E., & Baratta, G. A. 1995a, *Nature*, 373, 405
- Westley, M. S., Baragiola, R. A., Johnson, R. E., & Baratta, G. A. 1995b, *Planet. Space Sci.*, 43, 1311